(Received 2 December 2024, Accepted 27 February 2025, Scheduled 1 April 2025)

Rain Attenuation Modelling Based on Symbolic Regression and Differential Evolution for 5G mmWave Wireless Communication Networks

Sandra Bazebo Matondo* and Pius Adewale Owolawi

Department of Computer Systems Engineering, Tshwane University of Technology, Pretoria, South Africa

ABSTRACT: The microphysical structure of rain has a significant impact on the quality of radio signal transmission in the upcoming deployment of 5G millimetre-wave wireless communications in South Africa. To address this, mitigation techniques that integrate rain attenuation prediction models into network management systems are essential. This study uses a machine learning technique, symbolic regression coupled with differential evolution, to predict the rain attenuation in urban and rural 5G scenarios. Symbolic regression derives the mathematical models characterizing attenuation, while differential evolution optimizes the model coefficients. The models' accuracies are validated through predictive performance metrics, including Mean Absolute Error (MAE) and Mean Squared Error (MSE). The urban model showed excellent accuracy, and the rural model improved significantly after optimization. The interpretability of the models provides valuable insights into rain-induced attenuation and supports better design and optimization of 5G mmWave communication systems.

1. INTRODUCTION

Millimetre Waves (mmWaves) are radio waves with wavelengths between 10 mm (30 GHz) and 1 mm (300 GHz) [1, 2]. mmWave frequencies can be broadly categorized into sub-bands based on frequency ranges and applications as well as the balance they provide among bandwidth, propagation range, and penetration. For the initial deployment of the 5G mobile networks, the low band with a spectrum less than 1 GHz was chosen. The low-band spectrum offers a good balance between range and bandwidth and is suitable for long-range applications such as rural broadband access. The mid-band spectrum, which ranges from 1 GHz to 6 GHz, is the most popular band for 5G networks as it offers a satisfactory balance among range, capacity, and penetration. The third band (above 24 GHz), consisting of mmWave frequency spectrum, offers faster data rate capabilities and is suitable for applications that require extremely high data rates; however, it has a limited range and is more vulnerable to physical obstacles [3, 4].

In recent years, the deployment of 5G networks has been a significant success in solving the congestion problems in the lower radio frequency bands and in meeting the high demand from users for internet applications and services with higher data rates [1, 2, 5–7]. South Africa has implemented 5G technology primarily in lower frequency bands such as 700 MHz, 800 MHz, 2600 MHz, and 3.5 GHz. However, there is growing interest in using 5G mmWave technology to enable faster communication speeds and address congestion challenges associated with lower frequency bands.

Although mmWave frequencies offer desirable features in terms of connectivity, higher bandwidth, and spectral efficiency, as well as the ability to support higher data rates than 4G and lower 5G sub-bands, they suffer from free space channel degradation caused by factors such as weather conditions. Rain is one of the meteorological conditions that can scatter and absorb the radio signal transmitted in 5G mmWave links [3, 4, 8]. The feasibility of using frequencies in the mmWave spectrum for data transmission in 5G networks depends largely on local weather conditions. The frequent rain with heavy rainfall during South Africa's hot and humid summers severely affects 5G connectivity. The signal transmission power may be greatly reduced, affecting the quality of the signal or even leading to connection failures and deterioration of the Signal-to-Noise Ratio (SNR) of the 5G connection [8–10]. To maintain the desired SNR level, the power of the transmitted signals must be controlled considering the expected rain attenuation.

Symbolic Regression's (SR) ability to create easy-to-understand models and identify underlying mathematical relationships in the data makes it the preferred machine learning technique for modelling. SR simultaneously searches for the ideal model structure and parameters, unlike traditional regression techniques that assume a specific model structure. Many machine learning models, such as neural networks and support vector machines, act as "black boxes" and provide only limited insight into their decision-making processes.

While symbolic regression may not perform as well as deep neural networks on high-dimensional datasets [11], it offers a significant advantage in interpretability by generating mathematical equations as outputs. This property makes it partic-

* Corresponding author: Sandra Bazebo Matondo (bazebosm@gmail.com).

ularly useful in scientific research and engineering contexts. Additionally, symbolic regression has demonstrated its effectiveness in various fields, including biology and physics, where it is crucial to uncover the fundamental principles behind the data [12, 13].

In addition, the large search space offered by evolutionary algorithms commonly used in symbolic regression promotes population diversity and helps identify better models and their parameters. This in turn supports comprehensive analysis to achieve optimal accuracy and interpretability based on the problem requirements. In this work, a model that combines symbolic regression and Differential Evolution (DE) is proposed to build a robust rain attenuation prediction model for 5G mmWave links. The paper investigates the effectiveness of using DE and SR to model and predict rain-induced attenuation on the 5G mmWave terrestrial.

Symbolic regression is employed to derive a clear mathematical representation of the relationship between attenuation and essential variables, including frequency, rainfall rate, and path length. DE is used to optimize the model parameters estimated by SR. To address 5G millimetre-wave links, two prediction models are developed that represent urban and rural scenarios. The performance, especially in rural settings, is enhanced by applying differential evolution techniques to optimize the model further.

SR is a subset of machine learning that focuses on discovering a mathematical representation or equation for a given data set by integrating mathematical operations with the variables and constants involved in evolutionary processes [14]. DE [15] is a meta-heuristic evolutionary strategy that operates on a population of potential solutions that simultaneously search global space, balancing exploration and exploitation. DE is a suitable optimization technique to predict complex scenarios [16], such as the impact of machine learning features. Optimal attenuation values are achieved by tuning the SR-based predictor parameters with DE. The purpose of DE optimization is to minimize the error and allow the target values to converge with the predicted attenuation.

The focus is on outdoor line-of-sight (LoS) and non-line-of-sight (NLoS) propagation paths with rain attenuation. Moupfouma rain attenuation model [17] is used to produce the target attenuation values used in the model.

2. IMPACT OF FREQUENCY, PATH LENGTH AND RAIN RATE ON MMWAVE RAIN ATTENUATION

The size of a raindrop is comparable to the mmWave frequency wavelength. Therefore, raindrops act as obstacles, leading to the absorption and scattering of the propagating electromagnetic waves, resulting in signal degradation [3, 18, 19]. The attenuation caused by rain is influenced by the amount of rainfall accumulated in a given period. A high rain rate increases the number of raindrops, which in turn increases the probability of absorption, diffraction, and scattering [19, 20].

Additionally, the impact of rain attenuation on mmWave links can vary depending on factors such as the operating frequency, the distance between the transmitter and receiver, and the characteristics of the rain. The wavelength of the radio wave decreases as the frequency increase [19, 21]. The relatively large raindrops can cause significant scattering and absorption in the 5G links operating at mmWave spectrum than 5G links operating at lower frequencies [20, 21]. The distance between the receiver and transmitter is crucial in determining the attenuation caused by rain. The greater the distance is between the transmitter and receiver, the more raindrops the signal encounters. Each raindrop reduces the signal by a certain amount, increasing the risk that the signal will weaken over time.

This work will consider four different types of rain relevant for South Africa [22]. Table 1 shows different types of rain in South Africa and their rainfall rate characteristics at 1 min integration time.

TABLE 1. South Africa's rain rates categories [22].

Rain type	Rain rate at 1-min
Drizzle	$0.1\,\text{mm/hr} < R < 5\,\text{mm/hr}$
Widespread	$5\,\text{mm/hr} \leq R < 10\,\text{mm/hr}$
Shower	$10\,\text{mm/hr} \leq R < 40\,\text{mm/hr}$
Thunderstorm	$R \geq 40\,\text{mm/hr}$

Millimetre wave spectrum is critical not only for densely populated urban areas in South Africa, but also for expanding coverage in suburban and rural regions. Both microcells and macrocells are integral parts of a heterogeneous 5G network, with microcells serving as a key element in the mmWave 5G infrastructure. Microcells significantly increase network capacity in densely populated regions and, in combination with macrocells, form the backbone of 5G.

The proposed model is developed for practical 5G mmWave scenarios such as the Rural Macrocells (RMa), Urban Macrocells (UMa), and Urban Microcells(UMi) deployments as defined by the 3GPP TR 38.901 [23]. The study uses rain rate collected from 2013 to 2022. The 60-minute rain rate of various South African cities is converted to a 1-minute rain rate.

Attenuation will be predicted for 5G links operating at 5G mmWave frequency bands defined by 3GPP [23] as shown in Table 2.

TABLE 2. 5G mmWave frequency bands [23].

Bands	Uplink-downlink (GHz)	Frequencies (GHz)
n257	26.50–29.50	28
n258	24.5–27.50	26
n259	39.50–43.50	41
n260	37.00–40.00	39
n261	27.50–28.35	28
n262	47.20–48.20	47
n263	57.00–71.00	60

3. RELATED WORK

Many Machine-Learning (ML) based models have been proposed to predict the rainfall and attenuation on high frequency links. These predictions gave satisfactory results and presented a reasonable level of accuracy [24–27]. The authors in [25]

proposed an ML approach to predict rain fade and fog attenuation over time using data collected from geo-satellites in the 2.4–72 GHz range. Using neural networks, they were able to forecast the signal-to-noise ratio (SNR) several seconds in advance. The predicted SNRs were used to optimally adjust the signal strength. In [26], a model was proposed where Back-Propagation Neural Network (BPNN) was trained on 4 years rain data to predict rainfall rates. As a result, the study presented the attenuation that is likely to occur on the satellite link. An improved artificial neural network model to predict the rain attenuation for frequencies higher than 10 GHz was presented in [24], whereas in [28], an adaptive backpropagation in batch mode was used to accelerate the convergence during the training process. Authors in [27] predicted rain rate and attenuation at Ka- and Q-bands using Artificial Neural Network (ANN) models trained with Levenberg-Marquardt (LM) and Bayesian Regularization (BR) algorithms and long short-term memory (LSTM) network.

Symbolic regression is a growing field with fewer publications than more traditional regression and ML methods. However, its ability to develop interpretable models without sacrificing accuracy makes it increasingly popular in modelling wireless communication channels [29–33], where mathematical clarity is essential. In [29], researchers investigated the combination of SR techniques with transformer models to extract unique mathematical relationships. This approach has shown that SR can capture the complex behaviour of Terahertz waves in free space, facilitating high-speed transmission of satellite data while avoiding the complexity often associated with neural network-based models. The results of the study highlight the ability of SR to address the common challenge of balancing model complexity with interpretability, particularly when modelling high-frequency channels. Authors in [31] proposed a curved bridge prediction model using two unique branches of the SR technique, multigenic Genetic Programming (GP) and multi-biogeography-based programming. These models take into account mechanical, geometric, structural, and seismic parameters. The evolutionary correlation coefficient is used to determine the most important factors for seismic loads on bridge components. The resulting explicit models provide fast and reliable predictions without further simulation or assumptions for seismic demand models. In [34], four formulas which reproduced the correct physical law that governs the thermal conductivity of the grid were produced by genetic programming-based SR approach. The SR based model outperformed traditional models such as Debye-Callaway and Slack models.

While SR offers many advantages, it also has some disadvantages such as over-fitting problems and computational complexity. Moreover, SR searches for a vast space of possible mathematical expressions. This vastness makes it difficult to explore the entire space and ensure that the absolute best solution is found. A hybrid approach obtained by combining SR with other techniques can leverage the predictive strength of SR. Combining machine learning techniques and evolutionary algorithms is a promising solution to optimize computational efficiency and performance of machine learning techniques [35]. In [34], a gradient free method was proposed where Genetic Algorithm (GA) was used to evolve Convolutional Neural Networks (CNNs) weights. In [36], DE was successfully used for training ANNs. In [37], DE was used to train CNNs. Overall, the use of SR in prediction tasks offers a promising avenue for uncovering hidden patterns, generating accurate predictions, and gaining deeper insights into the underlying processes driving the data. As the demand for interpretable and flexible predictive modelling continues to grow, SR stands out as a valuable tool to predict the rain induced attenuation.

4. SYMBOLIC REGRESSION

SR identifies the relationship between a dependent variable y and a set of independent variables represented by a vector X. For a data set (X, y), a mathematical expression $f : \mathbb{R}^n \to \mathbb{R}$ is obtained such that $f(X_i) \approx y_i$, where each point $X_i \in \mathbb{R}^n$ and $y_i \in \mathbb{R}$. The expression tree structure is employed to facilitate the execution of evolutionary processes.

The goal of using SR is to find a mathematical expression that predicts rain attenuation in 5G mmWaves in urban and rural environments in South Africa based on the input data. Classic risk minimization is used to define the problem [38]. The search method used to discover the symbolic equation is Genetic Programming (GP). The search space in symbolic regression consists of numerous potential mathematical expressions. The evolutionary algorithms utilized in SR focus on efficiently searching and optimizing within this diverse space.

In this work, SR models are derived directly from the available data. The simulations are conducted using HeuristicLab and Matlab.

4.1. Genetics Programming

Symbolic regression begins by creating an initial random population of trees, denoted as $\mathcal{T}^{(0)}$, which then goes through an evolutionary process that includes mutation, crossover, and selection. Through this process, genetic programming iteratively improves solutions until a predefined stopping criterion is met. The final output is the set of selected expression trees represented by $\mathcal{T}$. The GP function class defines the search space, complexity, and balance between simplicity and precision, affecting the efficiency of the resulting equation. The function enables the generation of mathematical expressions using evolutionary processes.

Evolutionary processes occur sequentially and are aimed at preparing populations for subsequent stages. The optimal solution, derived from both the parent and offspring populations, is transmitted to the next generation. As shown in Figure 1(a), the mutation process in GP introduces random variations in individuals or candidates by replacing a subtree of the candidate with a newly generated random subtree.

In the symbolic regression crossover process shown in Figure 1(b), content is exchanged between two candidates, often exchanging subtrees between them. During the selection phase, individuals are selected from the current population to advance to the following generation [14, 39]. The candidate with the

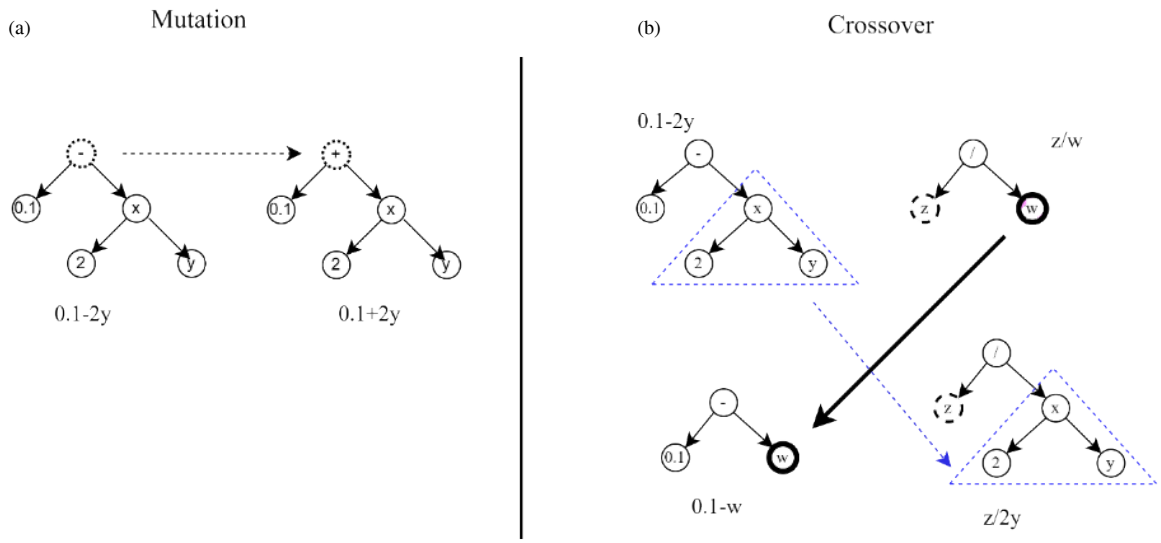

FIGURE 1. Mutation and crossover examples.

highest fitness score is prioritized for selection in the subsequent generation.

4.2. Model Input and Output Definition

The dataset is represented as $\mathcal{D} = \{(X_i, y_i)\}_{i=1}^{n}$ where $X_i \in \mathbb{R}^d$ is the input vector; $y_i \in \mathbb{R}^d$ is a scalar output; n denotes the total count of data points in the dataset. Figure 2 illustrates how SR is used to model rain attenuation.

$$A = f(R, F, D, c_0, c_1, \ldots, c_j) \tag{1}$$

Equation (1) represents the rain attenuation. A is a function of the rainfall rate $R_{0.01}$, operating frequency F, link distance (D), and model coefficients $(c_0, c_1, \ldots, c_j)$. The predicted rain attenuation $\hat{A}$, as determined by symbolic regression, is expressed as in Equation (2)

$$\hat{A} = f(R, F, D, c_0, c_1, \ldots, c_j) \tag{2}$$

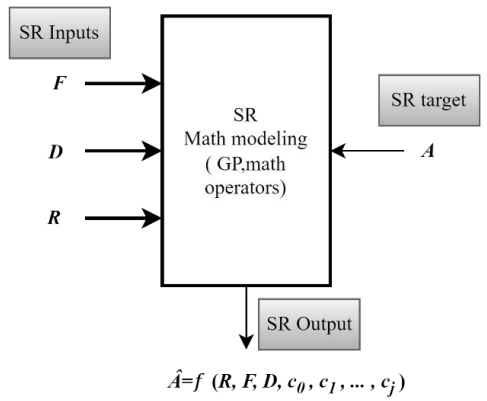

FIGURE 2. SR Modelling.

Using a data set V consisting of real-valued dependent and independent variables, where $V = \{R, F, D, A\}$, the output of the symbolic regression model (5.2) takes the form of Equation (3):

$$\hat{A} = f(V, c_0, c_1, \ldots, c_j) \tag{3}$$

The closed-form mathematical expression $f(V, c_0, c_1, \ldots, c_j)$ represents the model.

The SR process result is a model, or a set of models, that approximate the observed values of rain attenuation. This model should produce an estimate of the output $\hat{A}$, which is a function of the observed input variables. The predicted $\hat{A}$ should closely match the observed output A within a defined fitness criterion.

4.3. Loss Function

The loss function for each candidate $f \in \mathcal{F}$ which assesses the model's performance by measuring the difference between predictions and actual values is expressed in Equation (4).

$$l(f) = \sum_{i=1}^{n} l(f(X_i), y_i) \tag{4}$$

Mean Square Error (MSE) and Mean Absolute Error (MAE) are the common loss function used in regression problems. The mathematical equation for MSE is given in (5).

$$MSE = \frac{1}{n} \sum_{i} (y_i - \hat{y}_i)^2 \tag{5}$$

Here y_i and $\hat{y}_i$ represent the actual value and predicted value, respectively. The mathematical formula for MAE is shown in Equation (6).

$$MAE = \frac{1}{n} \sum_{i} |y_i - \hat{y}_i| \tag{6}$$

5. MODELS ANALYSIS AND RESULTS

In this section, the experimental results are presented, starting with a description of the data sets and experimental settings, followed by the simulation process. The model equations for urban and rural scenarios are then analysed, and their trends and the impact of various factors are discussed.

TABLE 3. Input features.

Scenario	UE-gNB range (km)	Frequencies (GHz)	Rain rate (mm/hr)
Rural Macro	0.035–5	28 26 41 39 28 47 60	$R_{0.01}$ 17–173.05
Urban (Micro and Macro)	0.01–0.3, 0.035–0.5		

5.1. Description of Datasets and Experimental Setting

The simulation data set includes NR 5G frequency bands, the distance between UE and gNB (considering the UMi, UMa, and RMa scenarios), the rainfall rate ($R_{0.01}$) for various South African cities, and the corresponding estimated rainfall-related attenuation. Details of the input features can be found in Table 3. Models are created for both urban and rural scenarios based on the cell size or the distance between UE and gNB. The simulations use a data set containing 79,000 example combinations of distance, frequency and $R_{0.01}$.

The input data set is created by systematically combining the input features: distance (UE-gNB range), frequencies, and rainfall rate ($R_{0.01}$), as shown in Table 3. Each combination represents a specific scenario of rain rate, frequency, and distance appropriate for rural macro and urban micro/macro scenarios. Moupfouma [17] method is used to calculate the rain-induced attenuation $A_{0.01}$, which serves as the target output. Moupfouma [17] path attenuation $A_{0.01}$ model is mathematically represented as in Equation (7)

$$A_p = aR_p^b D_{eff} \tag{7}$$

aR_p^b represents the specific rain attenuation (dB/km) at percentage of time p. R_p is the rain rate at the corresponding percentage of time p. a and b are frequency and polarization dependent regression coefficients. D_{eff} is the effective path length over which the rain propagation is considered uniform.

$$D_{eff} = rd \tag{8}$$

r is the reduction factor coefficient and d the actual path length in km. r can be expressed as (9)

$$r = \frac{1}{1 + 0.03(\frac{p}{0.01})^{-\beta} d^m} \tag{9}$$

where m is a coefficient that depends on the path length d and the carrier frequency F in GHz.

$$m = 1 + 1.4 \times 10^{-4} F^{1.76} \log_e d \tag{10}$$

The coefficient β can be obtained as in the following equations:

$$\left.\begin{array}{l} d{<}50\,\text{km} \\ \beta = 0.45 \quad \text{for} \quad 0.001 \leq p \leq 0.01 \\ \beta = 0.6 \quad \text{for} \quad 0.01 \leq p \leq 0.1 \end{array}\right\} \tag{11}$$

$$\left.\begin{array}{l} d \geq 50\,\text{km} \\ \beta = 0.36 \quad \text{for} \quad 0.001 \leq p \leq 0.01 \\ \beta = 0.6 \quad \text{for} \quad 0.01 \leq p \leq 0.1 \end{array}\right\} \tag{12}$$

5.2. Simulations

The models are trained on the first 70% of the relevant data set. The GP parameters used in the SR process are listed in Table 4. To increase the probability of finding an optimal solution, the population size is set to 1000. Sixty generations are chosen as an appropriate balance between computational efficiency and thorough exploration of the search space. A crossover probability of 90% is used to facilitate the exchange of subtrees between parent and offspring expressions. Meanwhile, a mutation probability of 15% results in sufficient variability in the expression trees without changing their structural integrity. The training parameters are carefully chosen because they impact both the effectiveness of the search process and the balance between complexity and interpretability of the resulting model.

TABLE 4. Models' depths and lengths.

	Rural	Urban
Model depth	14	13
model length	43	33

5.3. Model Equations and Interpretation

Mathematical expressions in symbolic regression are structured as trees, where the nodes correspond to operators or functions, and the leaves represent variables. In terms of tree structure, the complexity of the generated model depends on the depth

and length of the tree. The depth is defined by the number of levels in the expression tree. As shown in Table 4, the urban scenario has a depth of 13 and a length of 33, whereas the rural scenario has a deeper tree with 14 levels and a length of 43. As a result, the urban model is less complex in terms of both depth and length than the rural model.

5.3.1. Mathematical Expressions

In both models: A is the rain attenuation in dB; R is the rain rate (mm/hr); F is the frequency (GHz); D is the path length (km); and $c_0, c_1, c_2, \ldots, c_n$ are the model parameters defined by symbolic regression.

Rural scenario

The rural scenario mathematical expression is represented by Equation (13) which consists of two components A_1 and A_2, forming the total attenuation A as follows:

$$A = (A_1 + A_2) \cdot c_{18} + c_{19} \tag{13}$$

where:

$$A_1 = \log(c_0 D) \tag{14}$$

$$A_2 = c_1 R \left(\begin{array}{l} \frac{c_2 F - \frac{c_3 c_4 D}{c_5 F}}{c_6 - c_7} - (c_8 D + c_9 R) \\ \times \frac{c_{10} F - \frac{c_{11} - c_{12}}{c_{13} F}}{(c_{14} R)^2 + c_{15} R} - (c_{16} D + c_{17} R) \end{array} \right) \tag{15}$$

Equations (14) and (15) reveal that the interaction between the variables R, F, D, and rain attenuation is inherently nonlinear. Rain attenuation changes with variations in F, R, and D. In A_1, the term $\log(c_0 D)$ introduces nonlinearity, indicating that as D increases, its impact on A_1 decreases progressively. The terms in A_2 demonstrate a linear inverse relationship among distance D, frequency F, and rain rate R. Additionally, the inclusion of the inverse of R combined with F in the denominator contributes further nonlinearity to the model. Frequency F directly increases attenuation while simultaneously reducing the effect of distance D through inverse terms. Rain rate R has a linear impact on attenuation, as higher values of R lead to increased attenuation, particularly due to the $(cR)^2$ term. These interactions among the variables result in a nonlinear relationship governed by D, F, and R. Table 5 presents the symbolic regression parameters for the model.

Urban scenario

The mathematical expression derived from SR for the urban scenario is represented by Equation (16). This equation highlights the complex interaction among the three independent variables F, R, and D, with each playing a role in the overall signal attenuation.

$$A = \frac{c_0}{c_1} \frac{c_2 D}{\frac{c_3 F + \left(\frac{log(c_4 F)(c_5 R)^2}{c_6 c_7 F} - c_8 \right)}{c_9 D + c_{10} R . c_{11} F + c_{12} R}} (c_{13} + c_{14}) \tag{16}$$

In the rural model, distance D plays a major role with the attenuation increasing as D grows. Additionally, D amplifies the impact of both frequency F and rainfall rate R, intensifying their effects over longer distances. The attenuation also rises with the rain rate, primarily due to the nonlinear quadratic term $(c_5 R)^2$. Frequency F contributes to complex interactions by appearing in both the numerator and denominator, ultimately affecting attenuation through both linear and logarithmic terms such as $\log(c_4 F)$. The symbolic regression parameters specific to the urban model are detailed in Table 6.

The urban model exhibits the most intricate mathematical structure, characterized by its exponential reliance on distance, nonlinear relationships among all variables (distance, frequency, and rain rate), and several nested terms. In contrast, the rural scenario model is the least complex of the three but

TABLE 5. Rural scenario model parameters.

Parameters	Values
c_0	1.11950
c_1	0.10294
c_2	−0.21961
c_3	−17.27300
c_4	0.92089
c_5	0.02813
c_6	−8.33970
c_7	7.33120
c_8	3.67090
c_9	−0.03428
c_{10}	−0.06336
c_{11}	−8.25490
c_{12}	7.24640
c_{13}	0.26921
c_{14}	−0.01183
c_{15}	0.22893
c_{16}	3.03160
c_{17}	−0.002536
c_{18}	0.98177
c_{19}	−0.00677

TABLE 6. Urban scenario model parameters.

Parameters	Values
c_0	9.8158
c_1	−16.5770
c_2	1.7091
c_3	−0.3812
c_4	1.1731
c_5	0.2106
c_6	−4.0722
c_7	0.9622
c_8	8.3108
c_9	1.1403
c_{10}	1.7599
c_{11}	0.1393
c_{12}	−2.1916
c_{13}	0.8730
c_{14}	0.0059

still retains notable nonlinearity due to its fractional elements and quadratic components.

5.3.2. Analysis of Variable Impact

The study examines how input variables such as frequency, rain rate, and distance influence the performance and structure of the developed GP models. The variable impact highlights the key variables that enhance interpretability and identifies the most valuable features for optimizing the models. The findings for both scenarios are summarized in Table 7. The contribution of each input to the models is analysed based on their frequency of use, their impact on fitness, and interactions with other variables. While F, D, and R have comparable significance in all scenarios, frequency emerges as the most influential variable. This indicates that the model is most sensitive to frequency changes.

TABLE 7. Variables impact on the prediction models.

Input variables	Rural scenario	Urban scenario
F	0.419	0.433
D	0.292	0.305
R	0.289	0.263

Furthermore, signal attenuation is strongly influenced by propagation distance; as distance increases, more signal energy is absorbed or scattered, resulting in higher attenuation. Finally, rain intensity also plays a role, as higher amounts of precipitation lead to greater signal degradation.

5.3.3. Predictive Performance Analysis

The models' performance is assessed using metrics like MSE, MAE, and R^2, with the results detailed in Table 8.

For testing data set, R^2 scores of 0.999 and 0.996 were achieved for the rural and urban scenarios, respectively. These high scores demonstrate a strong correlation between the predicted and actual rain attenuation values. This strong alignment is further supported by the low MSE and MAE values observed. Among the scenarios, the rural model recorded the highest MSE value at 1.376, while the urban model achieved the lowest MSE at 0.02651. The MAE values for the urban and rural scenarios were 0.0976 and 0.8262, respectively. The performance metrics summarized in Table 8 confirm that the SR-based models effectively capture the relationships between the input variables (rain rate, frequency, and distance) and the target values (rain attenuation). During training, MSE and MAE were used to evaluate how well the models fit the data they were trained on. The lower MSE and MAE values recorded during testing indicate that the models generalize well to unseen data.

To ensure consistency in MSE values across data sets and models, normalized MSE (NMSE) is used. In the rural scenario, the test NMSE is lower than the training NMSE, indicating strong performance with additional data. While the test NMSEs for the urban and rural models are slightly higher than their training NMSEs, and they remain low, reflecting excellent generalization. On average, predictions for the rural and urban scenarios deviate by 23.73% and 4.31%, respectively. Figure 3 shows the comparison between urban predictions and targets at different distances and frequencies and at a rain rate of 168.05 mm/hr. Urban predictions closely match target values across all distances. Minor deviations are observed, with urban predictions slightly underestimating the attenuation at 26 GHz and 39 GHz. However, at higher frequencies (60 GHz), as the distance increases, urban predictions slightly overestimate the attenuation.

TABLE 8. Models' performance metrics.

	Rural	Urban
R^2 (training)	0.999	0.996
R^2 (test)	0.999	0.996
MSE (training)	1.450E+00	2.584E-02
MSE (test)	1.376E+00	2.651E-02
MAE (training)	8.394E-01	9.706E-02
MAE (test)	8.262E-01	9.764E-02
Average relative error (training)	22.42%	4.27%
Average relative error (test)	23.73%	4.31%
Normalized MSE (training)	1.222E-03	3.547E-03
Normalized MSE (test)	1.177E-03	3.713E-03

Figures 4–6 illustrate the comparison between the SR models' predictions and the target output at 28 GHz for an EU-gNB distance of 0.1 km.

Figure 6 compares the predicted attenuation values of different SR models with the actual target attenuation values at different rain rates. The SR models tend to underestimate attenuation, especially at higher rain rates. Figures 4–6 show that the urban model best matches the target values. While the urban scenario slightly overestimates the attenuation for rainfall rates between 20 mm/hr and 100 mm/hr, the urban model converges better with target values at higher rainfall rates. Conversely, the rural scenario significantly underestimates attenuation across almost the entire range of rain rates, making it the least accurate model as it predicts consistently lower attenuation than the target.

Figures 7 and 8 illustrate attenuation predictions for various rain rates at 28 GHz and compare the SR models with existing attenuation models. A growing difference is observed between the International Telecommunication Union (ITU) model and the other models, as the rain rate increases. As shown in Figure 8, the urban model shows a closer agreement with the Moupfouma model at both low and high rain rates. The Crane model [40] follows a similar pattern to the Moupfouma model.

6. DIFFERENTIAL EVOLUTION OPTIMIZATION

The rural model presents remarkably higher errors than the urban model, highlighting its limited predictive accuracy. To mitigate this issue, Differential Evolution (DE) [15] is applied to reduce the error between the predicted and target outputs. The DE technique is utilized to optimize the constant parameters $c_0, c_1, c_2, \ldots, c_{20}$ of the rural scenario model [30]. SR model optimization is shown in Figure 9. $\hat{A}$ is the predicted attenu-

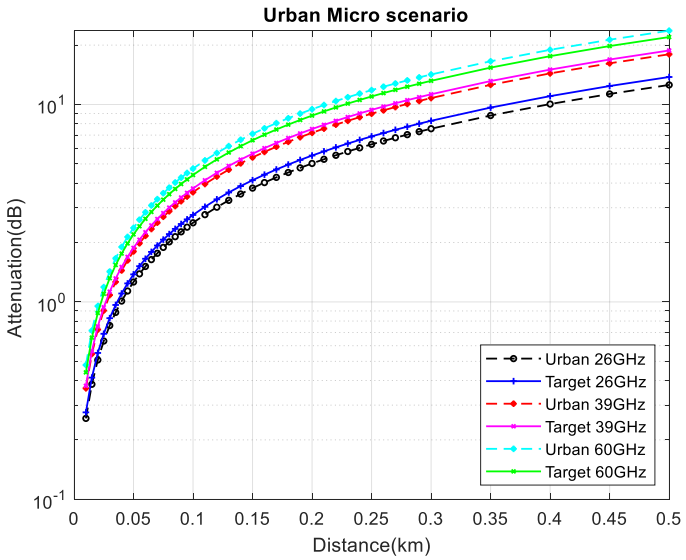

FIGURE 3. Impact of frequencies and distances in the urban scenario.

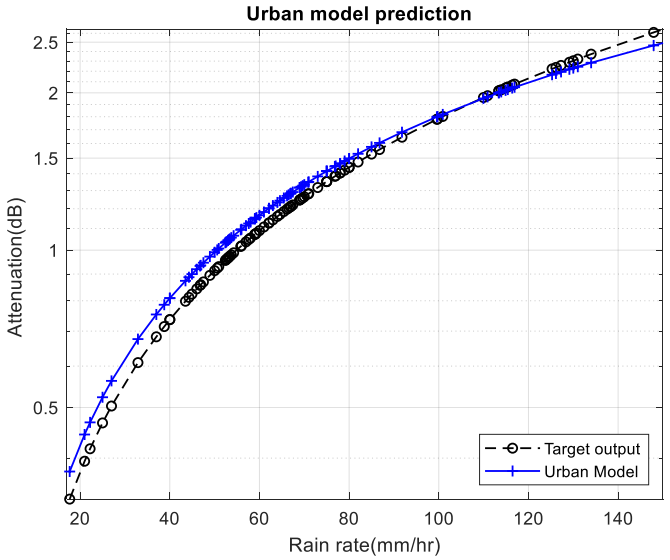

FIGURE 4. Attenuation predictions of urban scenario model.

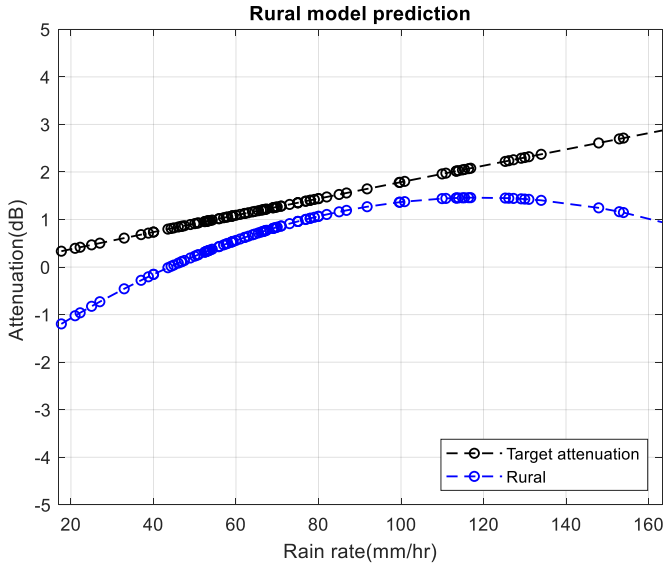

FIGURE 5. Attenuation predictions of rural scenario model.

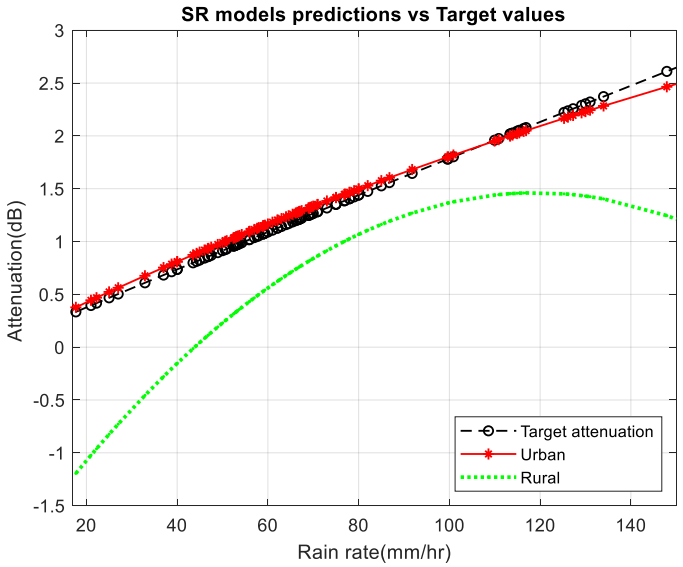

FIGURE 6. Comparison of the SR prediction models.

ation generated by the SR model and depends on the rainfall rate (R) exceeding 0.01% of the time, the operating frequency F, the link distance (D), and the model's constant parameters $(c_0, c_1, \ldots c_j)$. To further minimize the error between the actual values m and predicted values $\hat{m}$, the model coefficients $(c_0, c_1, \ldots, c_j)$ are refined using DE. Following DE optimization, the enhanced attenuation prediction $\hat{A}'$ is obtained as in Equation (17).

$$\hat{A}' = f(R, F, D, c'_0, c'_1, \ldots c'_j) \tag{17}$$

where $(c'_0, c'_1, \ldots c'_j)$ are optimal values of the constant parameters obtained through DE.

6.1. Differential Evolution Algorithm Description

In DE [15], the population of candidate solutions evolve through a sequence of operations, including mutation, crossover, and selection. Each operation prepares the population for the next generation. By merging the populations of parents and offspring, DE identifies the optimal solution, which is then carried forward to the next generation.

DE is employed to adjust the model parameters, to minimize the error between the predicted and actual attenuation values. The candidate solutions correspond to various sets of constant parameters c_0, c_1, c_2, …, c_{19} within the SR rural model. The optimization process, shown in Figure 10, achieves a balance between exploitation and exploration, facilitated by mutation and crossover. Exploitation is achieved through selection based on fitness and MSE. The optimization process starts by creating

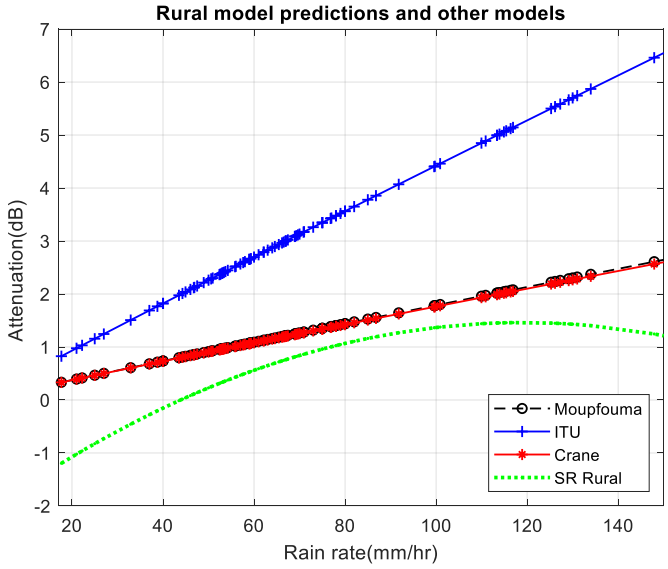

FIGURE 7. Comparison of SR rural model predictions with existing models.

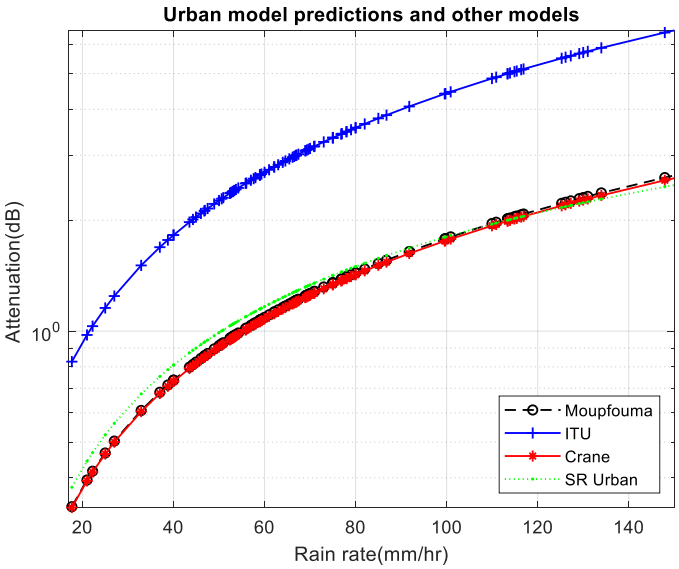

FIGURE 8. Comparison of SR urban model predictions with existing models.

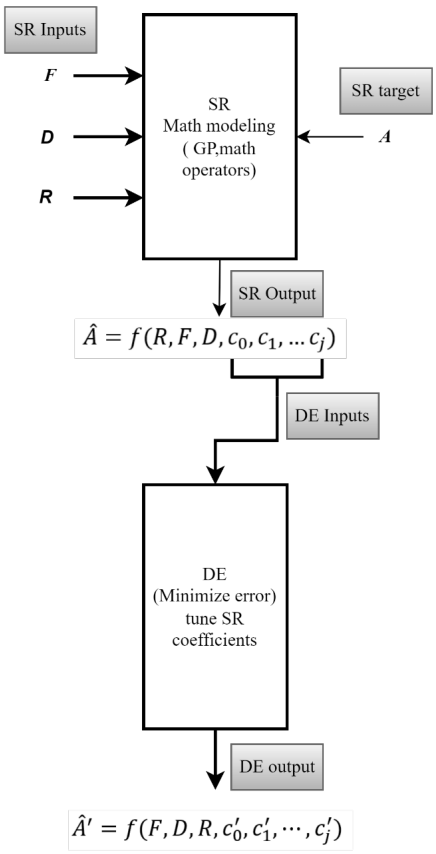

FIGURE 9. SR model optimization.

an initial population, $X = \{x_1, x_2, x_{3;\ldots}, x_p\}$ consisting of Np individuals. During the mutation phase, a new vector is formed by combining members of the current population. This process incorporates a mutation factor F and employs distinct random indices $r1$, $r2$, $r3$ to ensure diversity.

The crossover process generates a trial vector v_{ij}^G, where Cr denotes the crossover probability, and $rand_{ij}$ is a randomly generated number. The MSE is calculated as a cost function to evaluate the difference between the trial vector and target values. For the rural model, which includes a logarithmic expression, constraints are applied to ensure that all logarithmic parameters remain positive. The selection process identifies the optimal solution between the trial vector and current vector, and the algorithm continues to iterate until the cost function is below the threshold.

6.2. Objective Function

To minimize the error between the target outputs and predicted rain attenuation values, DE employs the mean square error (MSE) as its objective function, as defined in Equation (18):

$$MSE = \frac{1}{n}\sum_{i=1}^{n}\left(A_i - \hat{A}_i'\right)^2 \quad (18)$$

DE optimization minimizes the MSE, where A, $\hat{A}$, and n denote the target attenuation, predicted attenuation values, and the number of elements in the data set, respectively. DE optimization aims to minimize the MSE. By incorporating the independent variables and constant parameters, the objective function can be further expressed as shown in Equation (19):

$$MSE = \frac{1}{n}\sum_{i=1}^{n}\left(A_i - f(R_i, F_i, D_i, c'_0, c'_1, \ldots c'_j\right)^2 \quad (19)$$

Here, j indicates the number of coefficients in the SR model. After the optimization process, the DE produces an output as described in Equation (20).

$$\hat{A}' = f(F, D, R, c'_0, c'_1, \ldots, c'_j) \quad (20)$$

where $c'_0, c'_1, \ldots, c'_j$ represent the optimized parameters. This optimization significantly reduces MSE.

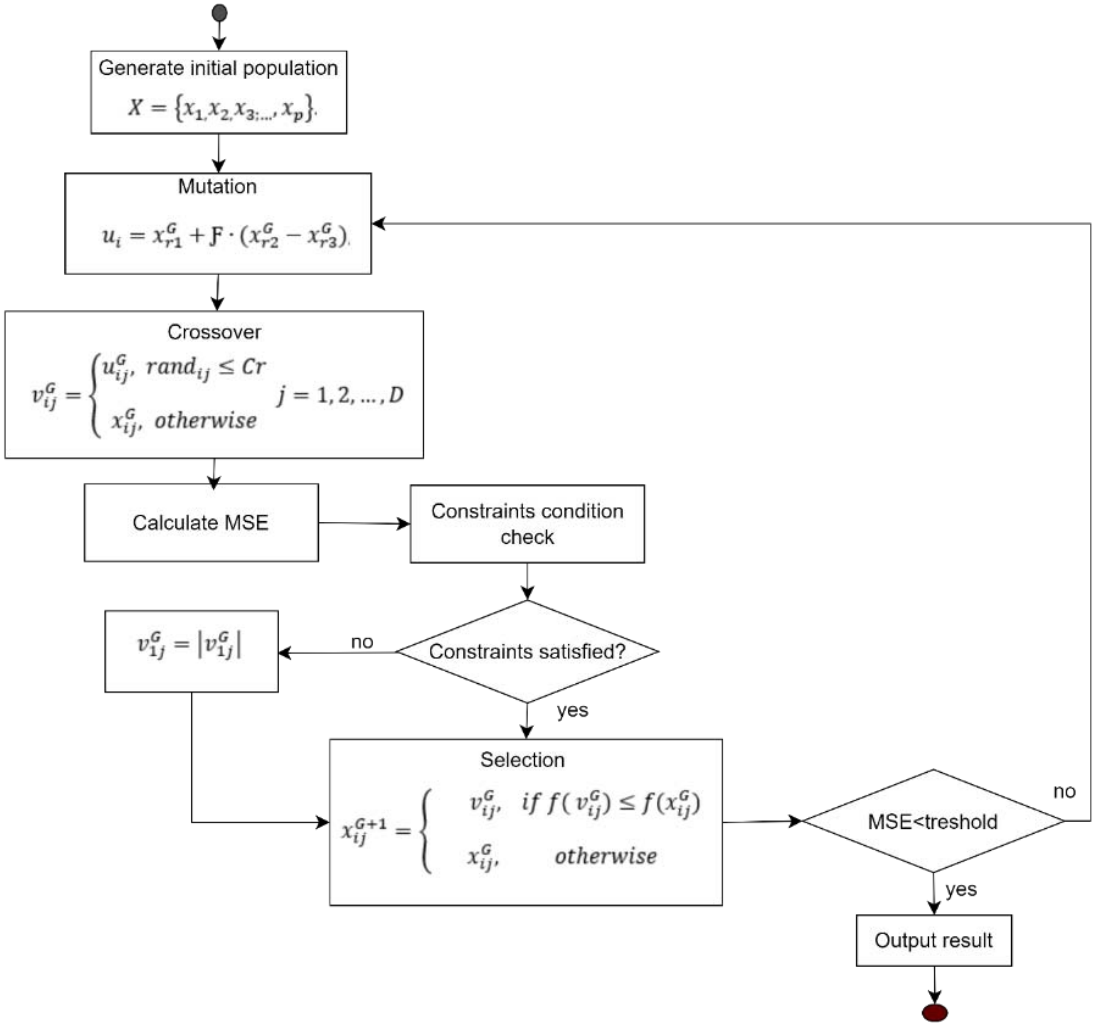

FIGURE 10. DE optimization algorithm.

6.3. Parameter Optimization Results

In the optimization process, each candidate solution x_i, in the population $X = \{x_1, x_2, x_{3;\ldots}, x_p\}$ consisting of Np individuals, is represented as a vector of *Npar* real numbers corresponding to the model coefficients c_0, c_1, . . ., c_{19} that require to be optimized. Over multiple generations, the DE algorithm minimizes the mean squared error (MSE) between the predicted attenuation (A) and observed attenuation ($\hat{A}'$), thereby determining the optimal values c_0, c_1, . . ., c_{19}.

In the simulation, the DE variant *rand/1/bin* is used. DE parameters are effectively configured to ensure a fast convergence and efficient search process. These settings include a population size $Np = 50$, mutation factor $f = 0.7$, crossover parameter $CR = 0.9$, and vector dimension $Npar = 20$. The optimized values of c_0, c_1, . . ., c_{19} obtained after applying DE are summarized in Table 9.

6.4. Analysis of Optimized Model

The optimization of the rural model led to significant changes in its parameters, including the reversal of several key terms and an increased influence of frequency F, distance D, and rain rate R. These adjustments altered the way these variables interact, making the model more responsive to changes in the input parameters. Notably, the model became much more sensitive to distance D, especially due to the logarithmic term in $A1$. The interactions among F, D, and R were also enhanced by significant changes in coefficients c_2 and c_3, while the overall scaling of the equation was adjusted by c_{18}. These optimizations led to improved prediction accuracy, making the model more applicable to real-world telecommunications systems. The performance metrics for both the rural and optimized rural models are presented in Table 10.

The optimized model demonstrates superior performance compared to the original rural model across all evaluation metrics. The MSE decreased from 1.3760 to 0.5011, reflecting a significant improvement in overall accuracy. The MAE dropped from 0.8262 to 0.3777, indicating a reduction in the average error magnitude. Moreover, the average relative error improved from 23.73% to 4.83%, showing a significant improvement in prediction accuracy. The normalized MSE also showed better error performance relative to the data size, decreasing from 1.177E-03 to 0.271E-3. In terms of both accu-

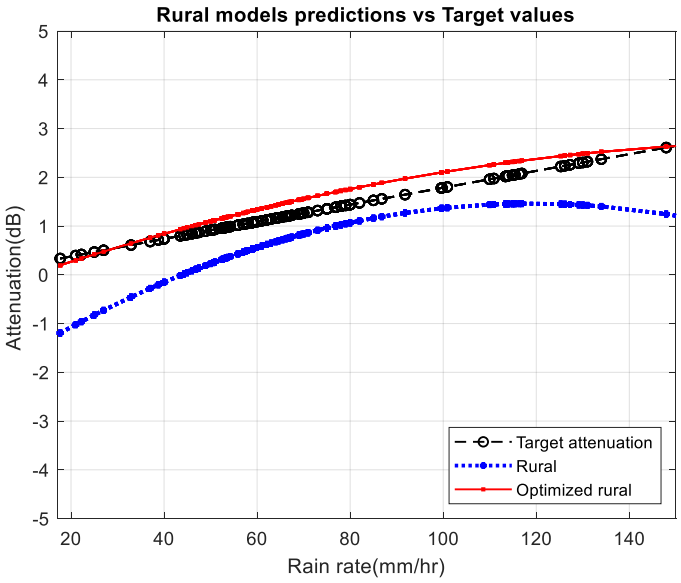

FIGURE 11. Comparison of optimized rural model with rural model.

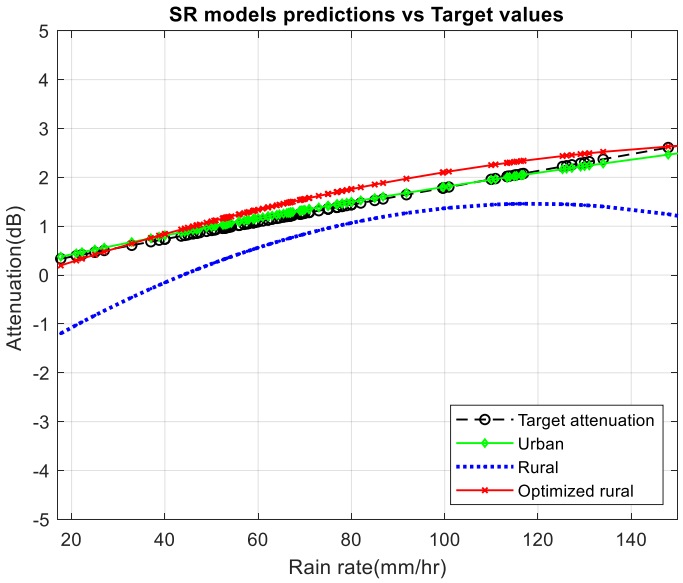

FIGURE 12. Comparison of optimized rural models with other SR models.

TABLE 9. Rural model parameters before and after optimization.

Parameters	Values	Optimized Values
c_0	1.11950	11.21581
c_1	0.10294	0.10562
c_2	−0.21961	−1.29614
c_3	−17.27300	19.91188
c_4	0.92089	−15.67390
c_5	0.02813	0.04434
c_6	−8.33970	13.36731
c_7	7.33120	−19.28980
c_8	3.67090	−5.75274
c_9	−0.03428	0.031442
c_{10}	−0.06336	−0.90165
c_{11}	−8.25490	−6.68869
c_{12}	7.24640	−15.11510
c_{13}	0.26921	−0.01524
c_{14}	−0.01183	−0.01811
c_{15}	0.22893	0.90423
c_{16}	3.03160	17.21333
c_{17}	−0.002536	−0.00520
c_{18}	0.98177	−0.17339
c_{19}	−0.00677	−0.43503

racy and error reduction, the optimized model significantly outperforms the original rural model.

Figure 11 illustrates the comparison of attenuation predictions as a function of rain rate. The original rural model consistently underestimates the attenuation across all rainfall rates, with a more noticeable discrepancy at higher and lower rain rates. In contrast, the optimized rural model's predictions align much more closely with the target attenuation, particularly where the original rural model shows more significant deviations. While the optimized model still slightly overestimates the target at rain rates, it more closely tracks the target's trend, providing a significant improvement in accuracy.

TABLE 10. Models' performance metrics.

Performance metric	Rural	Optimized rural
MSE	1.3760	0.5011
MAE	0.8262	0.3777
Average relative error	23.73%	4.83%
Normalized MSE	1.177E-03	0.271E-3

Figure 12 compares the optimized rural model with other SR models and the target attenuation across various rain rates. The attenuation predictions from both the optimized rural and urban models are nearly identical to the target, with the urban model performing slightly better. In contrast, the rural model significantly underperforms, particularly at higher and lower rain rates, where it consistently underestimates attenuation.

7. VALIDATION OF THE ADVANTAGES OF SR EQUATIONS

The SR equations derived from this work have brought significant benefits in terms of accuracy, interpretability, and insights into the physics of rain attenuation for 5G mmWave networks. Unlike traditional regression models, these equations reveal nonlinear dependence, dynamic interactions, and complex patterns of attenuation, balancing predictive performance with scientific understanding.

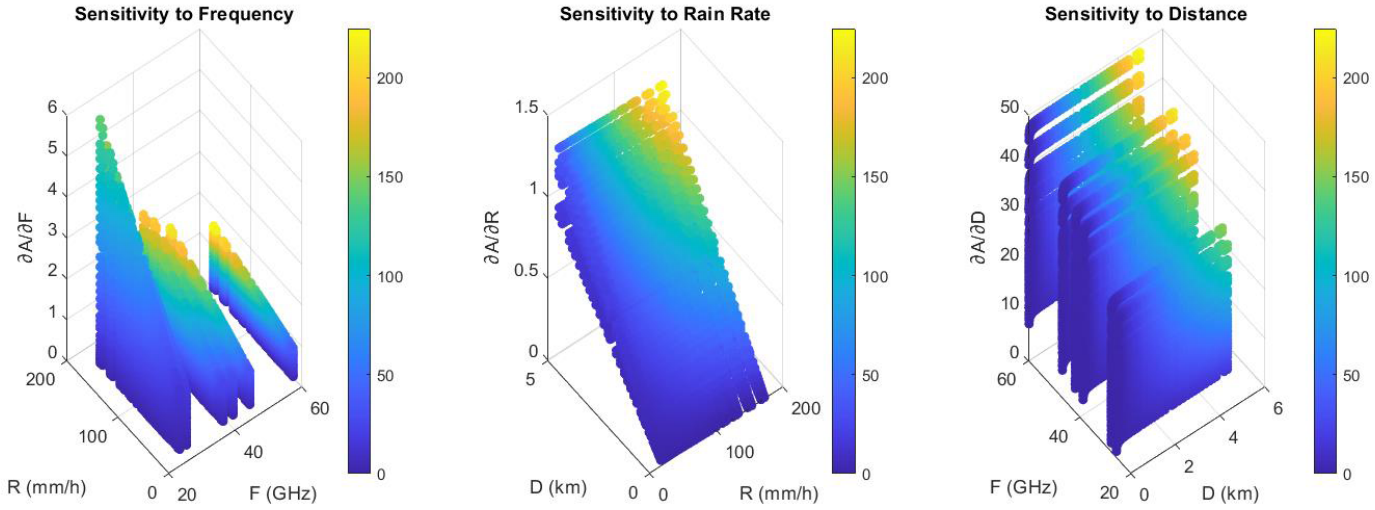

FIGURE 13. Sensitivity analysis optimized rural scenario.

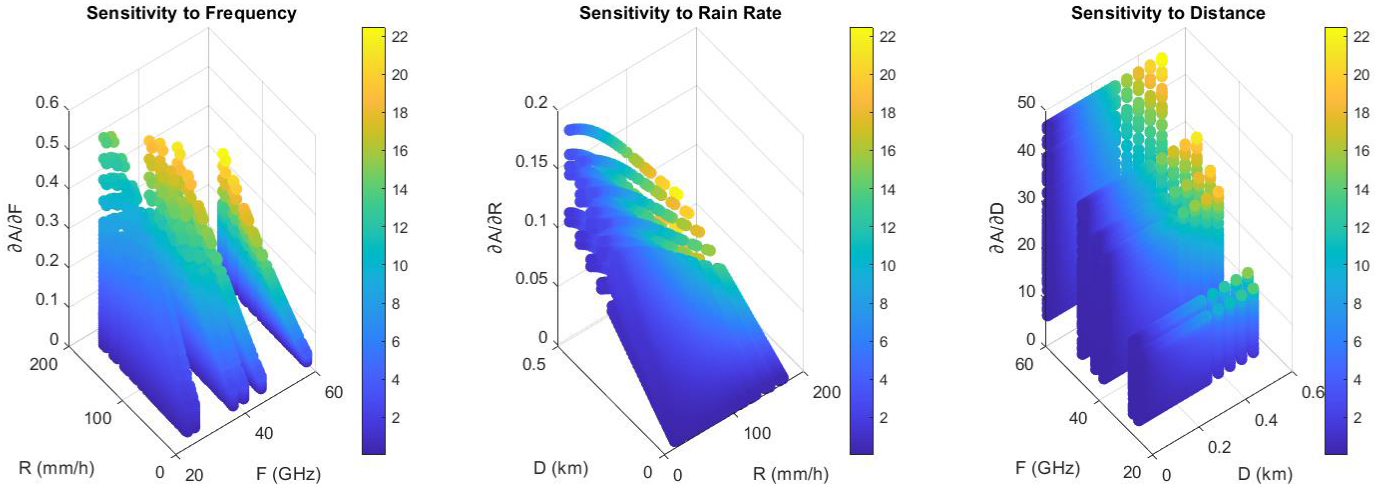

FIGURE 14. Sensitivity analysis urban scenario.

7.1. Uncovering Nonlinear Relationships and Discovering New Patterns

SR can effectively discover complex relationships between features, as demonstrated in [29] and [31]. Equations (13) to (16) illustrate such relationships among R, F, D, and A, through exponential, logarithmic, and polynomial interactions. The sensitivity analysis for the rural and urban scenarios is shown in Figures 13 and 14, where partial derivatives are computed to assess how A is sensitive to changes in R, D, and F. In both Figure 13 and Figure 14, A is highly sensitive to D. A small change in D significantly influences the values of $\partial A/\partial D$. In terms of sensitivity, the most important factor influencing attenuation is D, followed by F and then R.

Although the two scenarios show similar patterns, the rural scenario (Figure 13) has a more consistent relationship with rainfall and a steadier range of $\partial A/\partial R$ values. In contrast, the urban scenario (Figure 14) shows greater variability in rainfall sensitivity, indicating a less uniform response to changes in rain rate. In Figure 14, the rainfall has nonlinear effects on the attenuation, and its effect fluctuates in a nonlinear manner instead of increasing proportionally. The frequency sensitivity also indicates that F also exhibits nonlinear behaviour.

Attenuation results from combined effects, where the impact of one input variable is dependent on the values of the other input variables. Equations (13)–(16) show how attenuation depends on D, R, and F. However, their distinct mathematical structures result in different interactions among these variables. This suggests that they model attenuation with different levels of detail. For example, the logarithmic relationship with D in Equation (14) shows a unique distance relationship compared to Equation (16). The logarithmic distance relationship in Equation (14) indicates a decreasing rate of the attenuation increase, whereas the inverse frequency relationship demonstrates balancing effects. Equation (16), which introduces a squared R term, goes beyond the ITU power law's simple scaling and more accurately represents the nonlinear rain attenuation.

TABLE 11. Performance metrics of regression and SR-based models.

Model	MSE (Test)	MAE (Test)	R^2 (Test)
Polynomial Regression	33.81	5.73	−3.57
Linear Regression	1.01	0.67	0.863
Neural Network	0.002	0.0367	0.998
SR-Urban	0.530	0.380	0.999
SR rural + Differential Evolution	0.50	0.37	0.999

7.2. Improving Prediction Accuracy

As noted in [13], symbolic regression captures complex systems behaviour with high precision. Table 11 compares performances and shows that SR-Urban achieves significantly lower error rates than linear and polynomial regression models. While neural network achieves even lower error rates, SR offers a key advantage in interpretability by providing explicit equations instead of opaque black box models, as supported by [13]. Moreover, the integration of DE in SR improves the accuracy of Equations (13)–(15) and highlights the potential of DE to optimise predictive models, as proposed in [37].

7.3. Insights into Rain Attenuation Physics

The SR-based equations highlight the interdependence of R, F, and D in contrast to conventional rain attenuation models which rely on various multiplicative factors. This allows the predictions to be dynamically adapted to environmental conditions and shows that the attenuation is not strictly proportional to the intensity of rainfall but is also influenced by factors such as drop size distribution and atmospheric turbulence. The presence of logarithmic and rational frequency terms such as log(F) and F in both the numerator and denominator further emphasises the frequency-dependent absorption and scattering effects. This supports the idea that the attenuation varies with frequency in a more complex way than the ITU-R P.530 power-law relationship suggests. By capturing these complex relationships, SR-based equations can provide a more interpretable and physically grounded approach to rain attenuation modelling. The higher sensitivity of the SR models allows for a more accurate representation of the attenuation, especially in short-range scenarios where the conventional models may overlook small variations, as shown in Figure 8, where the SR model predicts the attenuation more accurately for all rainfall rates at shorter distances and is more accurate than the ITU model.

8. CONCLUSION

Rain attenuation is influenced by factors like frequency, rainfall rate, and link distance. Two models were developed using symbolic regression for 5G mmWave wireless communication networks in urban and rural scenarios. The urban mode showed strong performance, while the rural scenario model underperformed initially but improved through differential evolution optimization. DE optimization improved its prediction accuracy, minimized biases, and aligned with the urban model. The optimized model better captures the nonlinear relationship among rain rate, frequency, and distance, making it a more reliable tool for predicting rain attenuation in rural scenarios. The model's interpretability provides engineers and researchers with valuable insights into rain-induced attenuation in 5G mmWave wireless communication networks, enabling them to make more informed decisions when designing and developing 5G mmWave communication systems. These models have significant implications for improving network performance in various environments.

REFERENCES

[1] Rangan, S., T. S. Rappaport, and E. Erkip, "Millimeter-wave cellular wireless networks: Potentials and challenges," *Proceedings of the IEEE*, Vol. 102, No. 3, 366–385, 2014.

[2] Andrews, J. G., S. Buzzi, W. Choi, S. V. Hanly, A. Lozano, A. C. K. Soong, and J. C. Zhang, "What will 5G be?" *IEEE Journal on Selected Areas in Communications*, Vol. 32, No. 6, 1065–1082, 2014.

[3] Shamsan, Z. A., "Rainfall and diffraction modeling for millimeter-wave wireless fixed systems," *IEEE Access*, Vol. 8, 212 961–212 978, 2020.

[4] Narekar, N. P. and D. M. Bhalerao, "A survey on obstacles for 5G communication," in *2015 International Conference on Communications and Signal Processing (ICCSP)*, 0831–0835, Melmaruvathur, India, Apr. 2015.

[5] Bogale, T. E. and L. B. Le, "Massive MIMO and mmWave for 5G wireless HetNet: Potential benefits and challenges," *IEEE Vehicular Technology Magazine*, Vol. 11, No. 1, 64–75, 2016.

[6] Dahlman, E., S. Parkvall, and J. Skold, *5G NR: The Next Generation Wireless Access Technology*, Academic Press, 2020.

[7] Frenzel, L., "Millimeter waves will expand the wireless future," *Electronic Design*, No. 4, 30–36, 2013.

[8] Huang, J., Y. Cao, X. Raimundo, A. Cheema, and S. Salous, "Rain statistics investigation and rain attenuation modeling for millimeter wave short-range fixed links," *IEEE Access*, Vol. 7, 156 110–156 120, 2019.

[9] Shayea, I., T. A. Rahman, M. H. Azmi, and M. R. Islam, "Real measurement study for rain rate and rain attenuation conducted over 26 GHz microwave 5G link system in Malaysia," *IEEE Access*, Vol. 6, 19 044–19 064, 2018.

[10] Diba, F. D., M. A. Samad, and D.-Y. Choi, "The effects of rain on terrestrial links at K, Ka and E-bands in South Korea: Based on supervised learning," *IEEE Access*, Vol. 9, 9345–9355, 2021.

[11] Sandberg, L., "Astrophysicists Show How to "Weigh" Galaxy Clusters with Artificial Intelligence," Institute for Advanced Study, Princeton, NJ, USA, 2023.

[12] Kim, S., P. Y. Lu, S. Mukherjee, M. Gilbert, L. Jing;, V. Čeperić, and M. Soljačić, "Integration of neural network-based symbolic regression in deep learning for scientific discovery," *IEEE*

Transactions on Neural Networks and Learning Systems, Vol. 32, No. 9, 4166–4177, 2020.

[13] Makke, N. and S. Chawla, "Interpretable scientific discovery with symbolic regression: A review," *Artificial Intelligence Review*, Vol. 57, No. 1, 2, 2024.

[14] Koza, J. R., *Genetic Programming II*, MIT Press, Cambridge, 1994.

[15] Storn, R. and K. Price, "Differential evolution-a simple and efficient heuristic for global optimization over continuous spaces," *Journal of Global Optimization*, Vol. 11, 341–359, 1997.

[16] Das, S. and P. N. Suganthan, "Differential evolution: A survey of the state-of-the-art," *IEEE Transactions on Evolutionary Computation*, Vol. 15, No. 1, 4–31, 2010.

[17] Moupfouma, F., "Improvement of a rain attenuation prediction method for terrestrial microwave links," *IEEE Transactions on Antennas and Propagation*, Vol. 32, No. 12, 1368–1372, 1984.

[18] Ananya, S. T., M. S. Islam, M. A. R. Mahmud, P. K. Podder, and M. J. Uddin, "Atmospheric propagation impairment effects for wireless communications," *International Journal of Wireless & Mobile Networks (IJWMN)*, Vol. 12, No. 3, 45–61, 2020.

[19] Barclay, L. W., *Propagation of Radiowaves*, IET, 2003.

[20] Das, S., A. Maitra, and A. K. Shukla, "Rain attenuation modeling in the 10–100 GHz frequency using drop size distributions for different climatic zones in tropical India," *Progress In Electromagnetics Research B*, Vol. 25, 211–224, 2010.

[21] Nagaraj, P., "Impact of atmospheric impairments on mmwave based outdoor communication," *ArXiv Preprint ArXiv:1806.05176*, 2018.

[22] Afullo, T. J. O., "Raindrop size distribution modeling for radio link design along the eastern coast of South Africa," *Progress In Electromagnetics Research B*, Vol. 34, 345–366, 2011.

[23] 3GPP, "3rd generation partnership project technical specification group radio access network study on channel model for frequencies from 0.5 to 100 GHz (Release 18)," TR38.9012024, 98, 2024.

[24] Alencar, G. A., L. P. Caloba, and M. S. Assis, "Artificial neural networks as rain attenuation predictors in earth-space paths," in *Proceedings of the 2003 International Symposium on Circuits and Systems, 2003. ISCAS '03.*, Vol. 5, V–V, Bangkok, Thailand, May 2003.

[25] Domb, M. and G. Leshem, "Rain Attenuation Prediction for 2.4–72 GHz using LTSM, an artificial recurrent neural network technology," in *2021 International Conference on Electrical, Communication, and Computer Engineering (ICECCE)*, 1–6, Kuala Lumpur, Malaysia, Jun. 2021.

[26] Ahuna, M. N., T. J. Afullo, and A. A. Alonge, "Rain attenuation prediction using artificial neural network for dynamic rain fade mitigation," *SAIEE Africa Research Journal*, Vol. 110, No. 1, 11–18, 2019.

[27] Rao, D., D. Nandi, F. Pérez-Fontán, V. Pastoriza, and F. Machado, "Long term prediction of rain rate and attenuation using ANN and RNN algorithms," in *2021 IEEE International India Geoscience and Remote Sensing Symposium (InGARSS)*, 230–233, Ahmedabad, India, Dec. 2021.

[28] Sedki, A., D. Ouazar, and E. E. Mazoudi, "Evolving neural network using real coded genetic algorithm for daily rainfall-runoff forecasting," *Expert Systems with Applications*, Vol. 36, No. 3, 4523–4527, 2009.

[29] He, Y., B. Sheng, and Z. Li, "Channel modeling based on transformer symbolic regression for inter-satellite terahertz communication," *Applied Sciences*, Vol. 14, No. 7, 2929, 2024.

[30] Matondo, S. B. and P. A. Owolawi, "Impact of rain attenuation on short-range frequency operations in 5G networks," in *2024 25th International Microwave and Radar Conference (MIKON)*, 80–85, Wroclaw, Poland, Jul. 2024.

[31] Rezaei, H., P. Zarfam, E. M. Golafshani, and G. G. Amiri, "Development of seismic demand prediction models for bridges based on probability approach using symbolic regression method," *Computers & Structures*, Vol. 282, 106991, 2023.

[32] Loftis, C., K. Yuan, Y. Zhao, M. Hu, and J. Hu, "Lattice thermal conductivity prediction using symbolic regression and machine learning," *The Journal of Physical Chemistry A*, Vol. 125, No. 1, 435–450, 2020.

[33] Kolody, A.-H., E. Kabliman, J. Kronsteiner, G. Kronberger, and M. Kommenda, "Prediction of stress-strain curves for aluminium alloys using symbolic regression," in *ESAFORM Magazine*, 2019.

[34] Such, F. P., V. Madhavan, E. Conti, J. Lehman, K. O. Stanley, and J. Clune, "Deep neuroevolution: Genetic algorithms are a competitive alternative for training deep neural networks for reinforcement learning," *ArXiv Preprint ArXiv:1712.06567*, 2017.

[35] Galván, E. and P. Mooney, "Neuroevolution in deep neural networks: Current trends and future challenges," *IEEE Transactions on Artificial Intelligence*, Vol. 2, No. 6, 476–493, 2021.

[36] Baioletti, M., G. D. Bari, V. Poggioni, and M. Tracolli, "Differential evolution for learning large neural networks," 2018.

[37] Wang, B., Y. Sun, B. Xue, and M. Zhang, "A hybrid differential evolution approach to designing deep convolutional neural networks for image classification," in *AI 2018: Advances in Artificial Intelligence: 31st Australasian Joint Conference, Wellington, New Zealand, December 11-14, 2018, Proceedings 31*, 237–250, 2018.

[38] Vapnik, V., "Principles of risk minimization for learning theory," *Advances in Neural Information Processing Systems*, Vol. 4, 1991.

[39] Golberg, D. E., "Genetic algorithms in search, optimization, and machine learning. addion wesley," *Reading*, Vol. 673, 3, 1989.

[40] Crane, R. K., *Electromagnetic Wave Propagation through Rain*, Wiley, 1996.